

Hydrodynamic radial and elliptic flow in heavy-ion collisions from AGS to LHC energies

Gregory Kestin^{1,a} and Ulrich Heinz^{1,2,b}

¹ Physics Department, Ohio State University, Columbus, Ohio 43210, USA

² CERN, Physics Department, Theoretical Physics Division, CH-1211 Geneva 23, Switzerland

Abstract. Using ideal relativistic hydrodynamics in 2+1 dimensions, we study the collision energy dependence of radial and elliptic flow, of the emitted hadron spectra, and of the transverse momentum dependence of several hadronic particle ratios, covering the range from Alternating Gradient Synchrotron (AGS) to Large Hadron Collider (LHC) energies. These calculations establish an ideal fluid dynamic baseline that can be used to assess non-equilibrium features manifest in future LHC heavy-ion experiments. Contrary to earlier suggestions we find that a saturation and even decrease of the differential elliptic flow $v_2(p_T)$ with increasing collision energy cannot be unambiguously associated with the QCD phase transition.

1 Introduction

Relativistic hydrodynamics has proven to be very successful in describing the evolution of the hot and dense bulk matter created in heavy-ion collisions at the Relativistic Heavy Ion Collider (RHIC) [1,2,3,4]. Since, in the ideal fluid limit, it provides a direct connection between the equation of state (EOS) of the hot matter and the observed collective flow pattern that can be extracted from the measured hadron momentum spectra, this raised the hope of being able to constrain the QCD equation of state experimentally and to identify experimental signatures of the quark-hadron phase transition [5,6,7,8,9] which QCD predicts at high temperatures [10]. Specifically, ideal fluid dynamics predicts a non-monotonic collision energy dependence of the p_T -integrated elliptic flow v_2 [7], with a dip between SPS and RHIC energies caused by the softening of the QCD EOS around the quark-hadron phase transition. Unfortunately, large viscous effects during the late hadronic stage of the collision fireball expansion were found to spoil this phase transition signature [11,12], and experimentally the p_T -integrated elliptic flow was found to increase monotonically with collision energy [13,14] (see also [15,16]).

Contrary to the p_T -integrated elliptic flow, however, the PHENIX Collaboration found that the differential elliptic flow $v_2(p_T)$ for charged hadrons, at two fixed values of p_T ($p_T = 0.65$ and 1.75 GeV/ c), does not grow monotonically with increasing collision energy, but instead appears to saturate at RHIC in the center-of-mass energy range between 63 and 200 GeV/nucleon pair [17]. In Refs. [18,19,20] this observation was brought into connection with the QCD quark-hadron phase transition, speculating that the non-monotonicity of elliptic flow caused by the softening EOS near the phase transition, in spite of being washed out in the p_T -integrated v_2 , might survive viscous effects if measured at fixed p_T . This speculation was based on the observation that the monotonically increasing *radial* flow, which causes the transverse momentum spectra to fall off more slowly at higher collision energies, gives bigger weight to the high- p_T

^a e-mail: greg.kestin@gmail.com.

^b e-mail: heinz@mps.ohio-state.edu.

region (where $v_2(p_T)$ is larger than at low p_T) at high than at low collision energies, thereby counteracting in the p_T -integrated elliptic flow any reduction of $v_2(p_T)$ by a softening EOS. Any phase transition signature in the integrated v_2 should thus manifest itself even more prominently in the differential elliptic flow $v_2(p_T)$ at fixed p_T , and it might thus remain visible in the energy dependence of $v_2(p_T)$ even in the presence of viscous effects that smear out the signature in the p_T -integrated v_2 [18,19].

This conjecture remained speculative as long as there existed no systematic calculation of the collision energy dependence of the hydrodynamically generated differential elliptic flow. The present work fills this hole in the literature. Our study is based on ideal fluid dynamics even though the ideal fluid assumption is known to gradually break down below RHIC energies [18]. We do not attempt to quantitatively describe relativistic heavy ion data, but to provide theoretical insights into the systematics of the energy dependence of radial and elliptic flow within the ideal fluid picture. However, since the validity of the ideal fluid picture is expected to improve with increasing collision energy, providing an almost quantitative description of most low- p_T phenomena already at upper RHIC energies, the calculations presented here can be taken as a prediction for hadron spectra and their elliptic flow at LHC energies where effects from late hadronic viscosity are expected to become negligible [21]. As long as the viscosity of the quark-gluon plasma (QGP) stage (which at the LHC dominates over the hadronic one) remains sufficiently small, these predictions should give an accurate description of LHC data¹.

In addition to providing ideal fluid dynamical benchmarks for the LHC, an important finding of the present work is that a saturation and even decrease with growing beam energy of the differential elliptic flow $v_2(p_T)$ at fixed p_T cannot be unambiguously associated with the quark-hadron phase transition. We find that, at sufficiently high collision energies, $v_2(p_T)$ at fixed p_T *decreases* with increasing beam energy even when the matter is initially so dense that all elliptic flow is generated far above the phase transition and therefore not affected by the softening of the EOS near the critical temperature T_{cr} . This *decrease* of the p_T -differential elliptic flow at fixed p_T is accompanied by a simultaneous *increase* of the p_T -integrated elliptic flow. It is caused by an *increase of the radial flow* with growing beam energy which pushes the hadrons to larger p_T and renders the momentum spectra less anisotropic at low p_T . Our finding contradicts earlier speculations [18,19,20] and makes the task of identifying the QCD phase transition experimentally even more difficult than previously thought.

The present study is similar in spirit to and complements recent work by Niemi and Eskola *et al.* who also made ideal fluid dynamical predictions for hadron spectra [22] and elliptic flow [23] at LHC energies. Our analysis goes beyond theirs in its systematic investigation of the beam energy dependence of these hadronic observables.

2 Procedure

Our hydrodynamic simulations were performed with the (2+1)-dimensional hydrodynamic code AZHYDRO that solves the equations of motion in the two directions transverse to the beam direction for an ideal fluid undergoing boost-invariant longitudinal expansion [7,24,25]. To run the simulations we must initialize the program by providing the following parameters:

1. impact parameter b ;
2. initial proper time τ_0 at which the fluid is considered to be in local thermal equilibrium and the hydrodynamic expansion stage begins;
3. initial peak entropy density s_0 in central ($b = 0$) collisions: this parameter is used to control the final charged hadron multiplicity dN_{ch}/dy and serves as a proxy for the collision energy (see discussion below);

¹ As the beam energy and thus the initial fireball temperature T increases, the effective coupling strength $\alpha_s(T)$ decreases logarithmically; hence, the shear viscosity to entropy ratio η/s is expected to slightly increase from RHIC to LHC, suggesting stronger dissipative effects at the LHC. However, the particle density $n \sim T^3$ and mean free path $\lambda \sim 1/T$ vary much more rapidly with T ; correspondingly, the sound attenuation length $\Gamma_s = \eta/(sT)$ decreases from RHIC to LHC, and at any given time τ viscous effects, characterized by the ratio $\frac{\Gamma_s}{\tau} = \frac{\eta}{s} \frac{1}{T\tau}$, should be weaker at LHC energies than at RHIC.

4. peak value $n_{B,0}$ for the initial net baryon number density in central collisions: this parameter is used to control the finally observed anti-proton/proton ratio;
5. equation of state (EOS): we use an EOS that matches an ideal gas of quarks and gluons at a critical temperature $T_{\text{cr}} = 164 \text{ MeV}$ to a realistic hadron resonance gas with non-equilibrium hadron abundances whose chemical composition is frozen in chemical equilibrium at T_{cr} [24,26,27];
6. freeze-out temperature T_{dec} : this parameter controls where the hydrodynamic stage ends and how much collective flow builds up during the expansion. We use $T_{\text{dec}} = 100 \text{ MeV}$.

We simulate Au+Au collisions. The initial transverse entropy and baryon number density profiles are taken to be proportional to each other (constant entropy per baryon) and are calculated from the Glauber model with a mixture of soft and hard collisions, assuming 75% weight for the soft contribution, proportional to the transverse density of wounded nucleons, and 25% weight for the hard contribution, proportional to the transverse density of binary nucleon-nucleon collisions (see [2] for details). This mixture produces the correct centrality dependence of the charged hadron multiplicity at RHIC [2], and we assume that it doesn't change appreciably between RHIC and LHC. For the systematics of our study this is not a critical assumption. The initial transverse flow velocity at τ_0 is assumed to vanish.

In the absence of shocks, ideal fluid dynamics conserves entropy. Therefore, the observed charged hadron multiplicity dN_{ch}/dy , which measures the entropy of the final state, can be directly related to integral over the initial entropy density profile, parametrized by s_0 . Hydrodynamics cannot predict its own initial conditions, and a fundamental theory that reliably predicts the charged multiplicity as a function of collision energy \sqrt{s} does not exist yet. We therefore use dN_{ch}/dy or, equivalently, the initial peak entropy density in central Au+Au collisions, s_0 , as a proxy for the collision energy: At any given collision energy, a measurement of dN_{ch}/dy in the most central collision events fixes the value of s_0 to be used in ideal fluid simulations at that energy.

Using linear longitudinal expansion without transverse flow at very early times, dN_{ch}/dy and s_0 are thus related by

$$\frac{dN_{\text{ch}}}{dy} \propto \tau_0 \int d^2x_{\perp} s(\mathbf{x}_{\perp}, \tau_0) \propto \tau_0 s_0. \quad (1)$$

This relation involves two constants of proportionality, of which the first is the inverse of the average entropy per charged particle in the final state and is thus determined by the EOS at freeze-out, while the second depends on the shape of the initial entropy density profile which is fixed by the employed Glauber model. Equation (1) shows that s_0 and τ_0 are inversely proportional to each other. Since we vary the collision energy over orders of magnitude, the initial energy and entropy densities likewise vary by large factors. It is therefore not adequate to assume a constant thermalization time τ_0 independent of collision energy. Due to larger densities and temperatures at higher collision energies, thermalization should happen more rapidly. We assume that τ_0 scales with collision energy by satisfying a quantum mechanical uncertainty relation between the initial temperature T_0 (i.e. the initial average thermal energy) and the initial time τ_0 : $T_0\tau_0 = \text{const.}$ [28]. The constant is fixed by assuming the standard value $\tau_0 = 0.6 \text{ fm}/c$ at RHIC energies, $\sqrt{s} = 200 \text{ GeV}/\text{nucleon pair}$ (it turns out to be approximately 1 [2]). Since for all collision energies considered here the fireball center in $b = 0$ collisions is in the QGP phase, $s_0 \propto T_0^3$. Combining these relations with Eq. (1), one finds

$$\frac{\tau_0(\sqrt{s_1})}{\tau_0(\sqrt{s_2})} = \frac{T_0(\sqrt{s_2})}{T_0(\sqrt{s_1})} = \sqrt{\frac{dN_{\text{ch}}/dy(\sqrt{s_2})}{dN_{\text{ch}}/dy(\sqrt{s_1})}}, \quad \frac{s_0(\sqrt{s_1})}{s_0(\sqrt{s_2})} = \left(\frac{dN_{\text{ch}}/dy(\sqrt{s_1})}{dN_{\text{ch}}/dy(\sqrt{s_2})} \right)^{3/2}. \quad (2)$$

Figure 1 shows a compilation [29] of measured hadron multiplicities from $(A \approx 200) + (A \approx 200)$ collisions at a variety of collision energies explored at the AGS, SPS and RHIC, together with a linear fit in $\log_{10} \sqrt{s}$:

$$\frac{dN_{\text{ch}}}{d\eta} = 312.5 \log_{10} \sqrt{s} - 64.8 \quad (3)$$

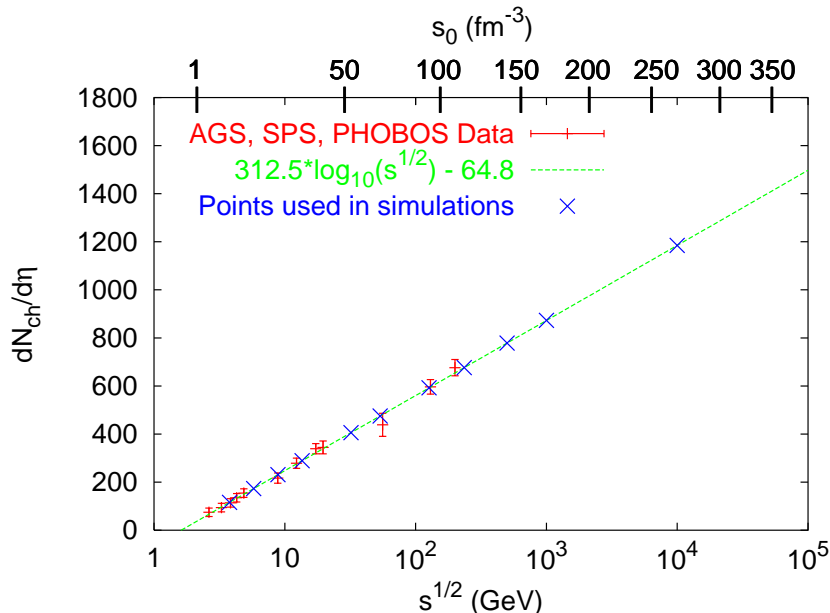


Fig. 1. (Color online) Charged particle multiplicity $dN_{ch}/d\eta$ vs. center of mass energy per nucleon pair \sqrt{s} (lower horizontal axis) and initial peak entropy density s_0 (upper horizontal axis). The experimental data are from central Au+Au and Pb+Pb collisions at AGS, SPS, and RHIC energies and were compiled in Ref. [29]. The dashed line is a linear fit to the data. Crosses indicate values for s_0 and $dN_{ch}/d\eta$ for which hydrodynamic simulations were performed. See text for details.

The upper horizontal axis maps the multiplicities on the vertical axis onto s_0 values, using Eq. (2) with $s_0(\sqrt{s}=200 \text{ A GeV}) = 117/\text{fm}^3$ [25,2]. The linear fit (3) provides guidance for which values to expect for $dN_{ch}/d\eta$ and s_0 at hitherto unexplored LHC energies. We emphasize, however, that s_0 is not directly related to \sqrt{s} , but only indirectly via Eq. (1) through the charged multiplicity measured at that value of \sqrt{s} . For this reason we have performed several “LHC simulations” with a variety of s_0 values within a reasonable range of the value predicted by the simple-minded linear extrapolation of existing data shown in Fig. 1. The first day of LHC heavy-ion experiments will tell us which of these simulations to choose as hydrodynamic reference for the data.

We finally comment on our choice of the initial peak net baryon density $n_{B,0}$. At RHIC energies it was fitted to the measured \bar{p}/p ratio to give $n_{B,0} = 0.44/\text{fm}^3$ at $\tau_0 = 0.6 \text{ fm}/c$. We did not attempt to fit the \sqrt{s} -dependence of $n_{B,0}$ from \bar{p}/p ratios measured at lower collision energies. Instead we simply held $n_{B,0} = 0.44/\text{fm}^3$ constant over the entire energy range while reducing τ_0 with increasing collision energy according to Eq. (2). This implies that, at fixed τ , n_B decreases with increasing multiplicity as $1/\sqrt{dN_{ch}/dy}$. Together with the increasing s_0 values, this leads to a significant (although perhaps not quite strong enough) decrease of the net baryon to entropy ratio at midrapidity. Correspondingly, the baryon chemical potential at chemical decoupling decreases, reflecting increasing nuclear transparency and decreasing baryon stopping power at higher energies. At our highest s_0 value, $s_0 = 271/\text{fm}^3$ (last cross in Fig. 1), we simply set $n_{B,0} = 0$, assuming approximate baryon-antibaryon symmetry at midrapidity at the LHC.

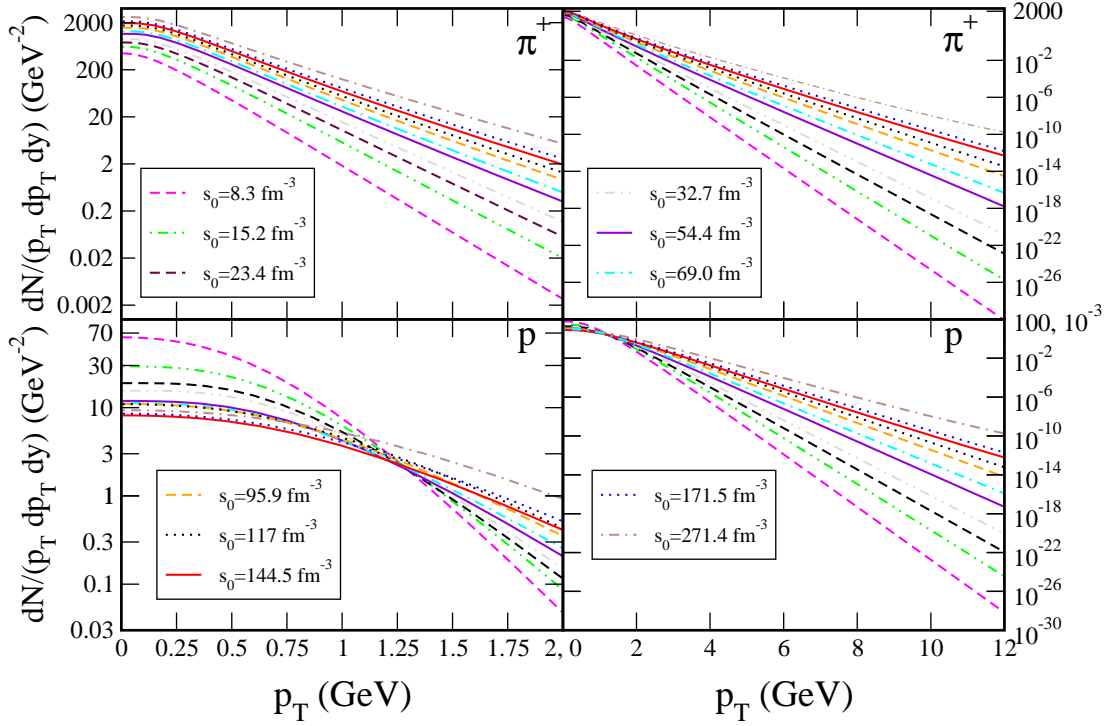


Fig. 2. (Color online) Transverse momentum spectra for thermal pions (π^+ , upper panels) and protons (p , lower panels) at low (left panels) and intermediate (right panels) values of p_T , for central Au+Au collisions with a variety of initial peak entropy densities s_0 .

3 Radial Flow

3.1 Transverse momentum spectra from AGS to LHC

Figure 2 shows the p_T -spectra for directly emitted π^+ mesons (upper row) and protons (lower row). In this plot we have neglected feed-down from resonance decays; its inclusion is computationally intensive but, since we keep T_{dec} the same at all collision energies, it will not qualitatively affect the systematics shown in Fig. 2. Here and in the following the curves are labelled by the value of s_0 . The reader can use Fig. 1 to translate this value into charged hadron multiplicities (which include resonance feeddown) and to estimate the corresponding collision energy.

The normalization of the pion p_T -spectra is seen to increase with s_0 , reflecting the growth of the total multiplicity with increasing collision energy. They also become systematically flatter as s_0 increases; since the decoupling temperature T_{dec} is held fixed, this is an unambiguous signature for larger radial flow at higher collision energies.

The radial flow effects on pion and proton spectra are similar at large transverse momenta (right panels in Fig. 2) where their rest mass difference can be neglected and the flow effect can be understood in terms of the simple blueshift formula $T_{\text{slope}} = T_{\text{dec}} \sqrt{\frac{1+\langle v_{\perp} \rangle}{1-\langle v_{\perp} \rangle}}$ [30,31]. At low p_T , however, they are much more pronounced for the heavier protons (lower left panel in Fig. 2) [30,31]. One sees that the radial flow pushes the protons away from $p_T = 0$, leading to both a dramatic flattening of the p_T -spectrum and a decrease of the proton yield at low p_T , in spite of the overall increase in multiplicity. (It should be mentioned that the decrease in proton yield at low p_T is amplified by the decrease of the baryon chemical potential at higher collision energies, but we checked that it is also visible in the antiproton spectra.) Only at the highest collision energies, where the low- p_T proton spectra are almost flat, the low- p_T proton yields are seen to follow the general increase in multiplicity.

3.2 p_T - and m_T -dependence of particle ratios: RHIC vs. LHC

Hydrodynamic radial flow, which leads to flatter p_T -spectra for heavy particles, is a key contributor to the observed [4] strong rise of the \bar{p}/π and Λ/K ratios at low p_T at RHIC [2]. The left column in the left panel of Figure 3 shows that this rise is predicted to be slower at the LHC than at RHIC. Since *all* spectra are flatter at the LHC due to increased radial flow (right column of the left panel) while their asymptotic ratios at $p_T \rightarrow \infty$ (given by their fugacity and spin degeneracy ratios [2]) remain similar, the ratios between the spectra increase more slowly with p_T .

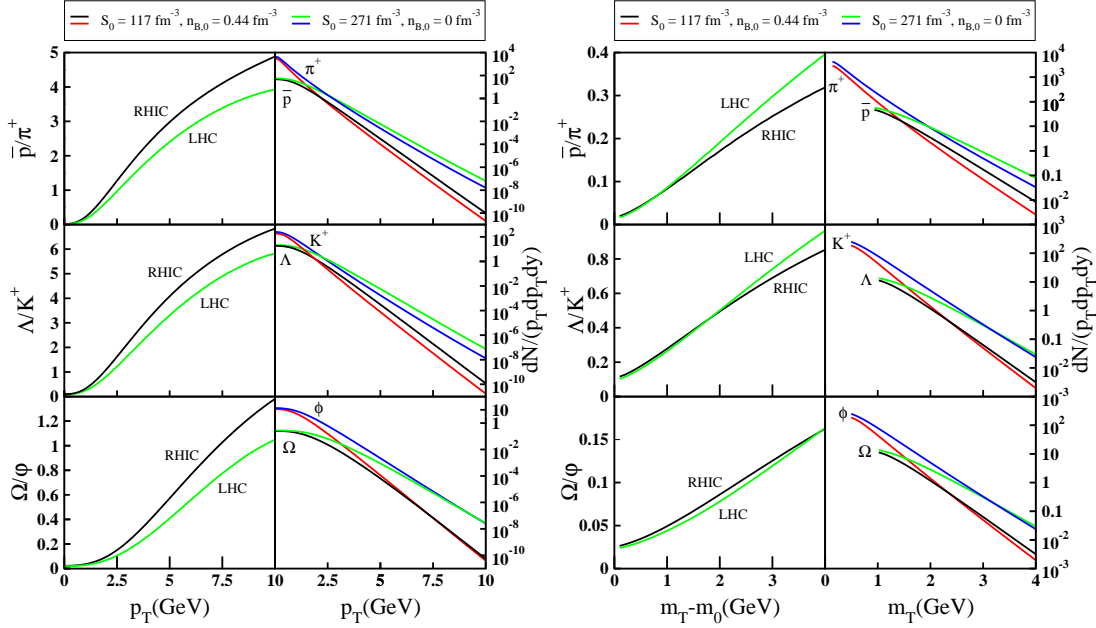


Fig. 3. (Color online) *Left panel:* Transverse momentum spectra (right half) and selected particle ratios (left half) as functions of p_T for central Au+Au collisions at RHIC and LHC energies (see text for details). A zoomed version of this plot which focusses on the region $p_T < 2$ GeV/c can be found in Fig. 53 of Ref. [32]. *Right panel:* Same as left panel, but plotted as a function of transverse mass m_T or transverse kinetic energy $m_T - m_0$, respectively, over the m_T range where hydrodynamics is expected to be a valid description. All curves shown in this Figure include the contributions from resonance decays.

In the right panel of Fig. 3 we redraw the curves shown in the left panel as a function of transverse mass m_T (for the spectra) or transverse kinetic energy $m_T - m_0$ (for the particle ratios). We do so in order to isolate flow effects, by eliminating the kinematic contribution to the rise of the p_T -dependent heavy/light hadron ratios that results from plotting thermal distributions (which depend on $\frac{m_T}{T_{\text{dec}}}$) as a function of $p_T = \sqrt{m_T^2 - m_0^2}$. In the absence of radial flow, the m_T -spectra would show perfect m_T -scaling, and (except for minor effects from resonance feeddown and Bose statistics for pions) the ratios between spectra of particles with different rest masses would thus be independent of m_T or $m_T - m_0$. The rise of the ratios shown in the left half of the right panel of Fig. 3 (which is much weaker than that in the left half of the left panel) can thus be attributed almost exclusively to radial flow effects. A comparison of future LHC data on $(m_T - m_0)$ -dependent heavy/light particle ratios with the hydrodynamical predictions shown in Fig. 3 can therefore help to separate collective flow effects from more exotic explanations such as “baryon junctions” [32].

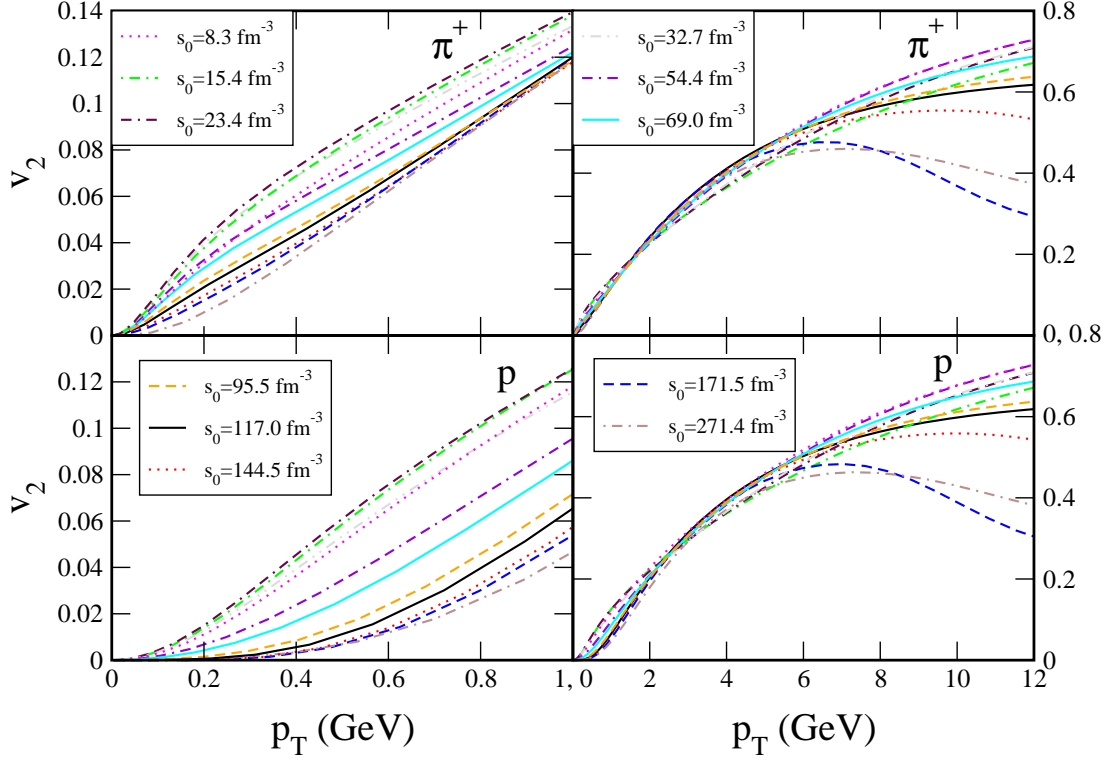


Fig. 4. (Color online) Differential elliptic flow $v_2(p_T)$ for directly emitted pions (π^+ , upper panels) and protons (p , lower panels) at low (left panels) and intermediate (right panels) values of p_T , for $b = 7$ fm Au+Au collisions with a variety of initial peak entropy densities s_0 .

4 Elliptic Flow

While ideal fluid dynamics begins to break down below RHIC energies, due to viscous effects in the late hadronic stage which persist even at RHIC [11,12], its validity is expected to improve at the LHC where the elliptic flow saturates in the QGP stage and effects from late hadronic viscosity become negligible [21]. Early viscous effects in the QGP stage seem small at RHIC [2,12], and recent results from Lattice QCD indicate little change of its specific shear viscosity η/s from RHIC to LHC [33]. The following *ideal fluid* dynamical predictions for soft ($p_T < 2\text{--}3$ GeV/ c) hadron production in ($A \approx 200$)+(A ≈ 200) collisions at the LHC should thus be quite robust.

In Figure 4 we look at the differential elliptic flow for both protons and π^+ as a function of transverse momentum for $b = 7$ fm Au+Au collisions at various collision energies. The left panels are expanded views of the low- p_T end. At all collision energies, over 99 percent of all particles are emitted with transverse momenta below 1.5 GeV/ c ; for this reason we focus our attention on the system's characteristics at low p_T .²

By scanning the curves in order of increasing s_0 one notices for both pions and protons that, at low p_T , the differential elliptic flow at fixed p_T is not monotonic with collision energy.

² The astute reader may be puzzled, as we were initially, by the fact that, for the highest collision energies studied here, the elliptic flow peaks at intermediate p_T and then decreases again, instead of monotonically increasing with p_T . This effect appears to be caused by the following phenomenon: even though *on average* the hydrodynamic flow at freeze-out is stronger in the reaction plane than perpendicular to it, at high collision energies the *largest* value of the flow velocity is found on the freeze-out surface in out-of-plane direction. Since the highest- p_T hadrons are emitted from fluid cells with the largest flow velocities, this causes a reduction of v_2 at very high p_T , causing it eventually to even turn negative [34]. We thank P. Huovinen for a clarifying discussion on this point.

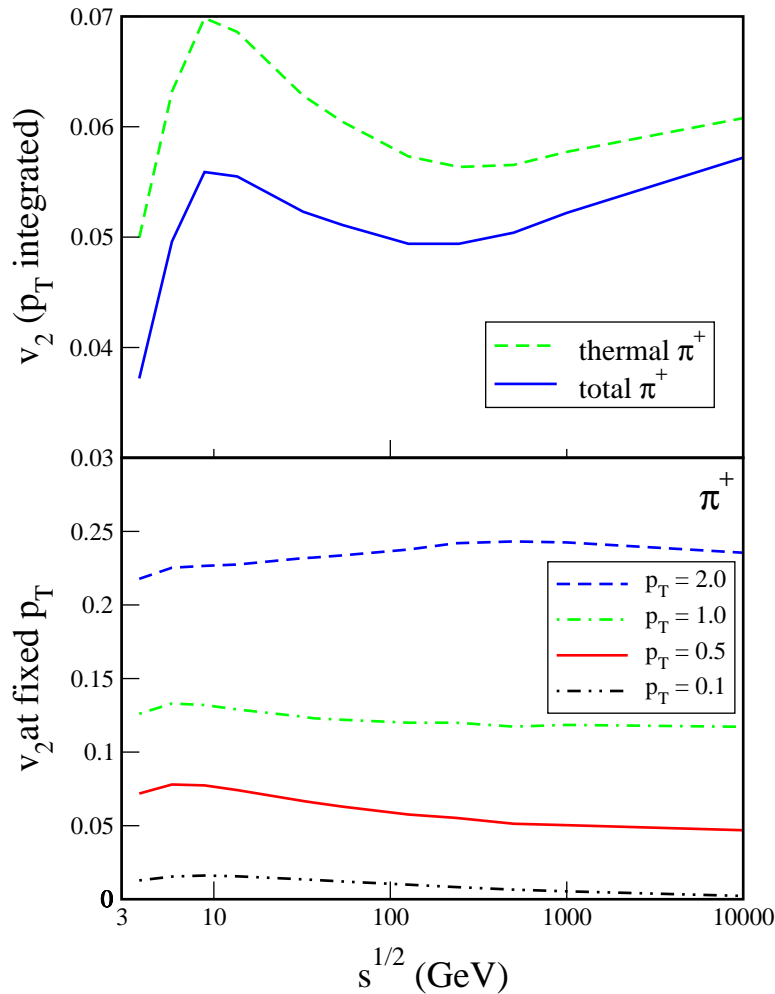


Fig. 5. (Color online) *Upper panel:* p_T -integrated elliptic flow for pions from $b = 7$ fm Au+Au collisions as a function of collision energy, assuming the relation shown in Fig. 1 between s_0 and \sqrt{s} . The solid line takes only directly emitted thermal pions into account, the dashed line includes pions from resonance decays. *Lower panel:* Energy dependence of thermal pion elliptic flow from $b = 7$ fm Au+Au collisions at four fixed values of p_T (in GeV/ c), as indicated.

At the low-energy end $v_2(p_T)$ first increases with s_0 , but when the collision energy is further increased beyond $\sqrt{s} \geq 10$ GeV/nucleon pair, the differential elliptic flow decreases again.

This is explored more quantitatively in the lower panel of Fig. 5 which shows the differential elliptic flow of directly emitted pions at fixed p_T as a function of \sqrt{s} (using the fit in Fig. 1 to translate s_0 into \sqrt{s}), for four different p_T values. The three curves corresponding to $p_T = 0.1, 0.5$ and 1 GeV/ c all show this non-monotonic behavior of a $v_2(p_T)$ that first rises and then decreases with collision energy. The increase at low \sqrt{s} values is easy to understand: at low collision energies, the fireball decouples before the elliptic flow can saturate; by increasing the collision energy, the fireball lifetime is increased, allowing the elliptic flow to grow and reach values closer to its asymptotic saturation value. Between SPS and RHIC energies, the fireball lifetime is sufficiently long for the elliptic flow to more or less saturate [7]. The explanation for the decrease of $v_2(p_T)$ at higher energies is more subtle: As the collision energy increases further, the magnitude of the *radial* flow continues to grow, too, leading to ever flatter p_T -spectra. Flatter p_T -spectra show less azimuthal variation and thus exhibit smaller v_2 coefficients [35].

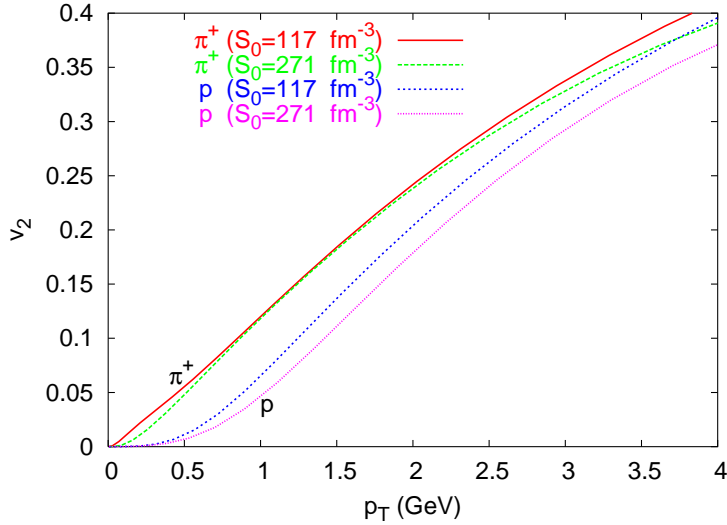


Fig. 6. (Color online) Differential elliptic flow $v_2(p_T)$ for thermal pions and protons from $b = 7$ fm Au+Au collisions at RHIC ($s_0 = 117 \text{ fm}^{-3}$) and LHC ($s_0 = 271 \text{ fm}^{-3}$) energies, plotted together for comparison.

This flattening effect of radial flow on the p_T -spectra is particularly pronounced at low p_T (see Fig. 2). This may explain why the non-monotonic beam energy dependence of $v_2(p_T)$ is only seen at low p_T up to about $1 \text{ GeV}/c$ and seems to disappear above $p_T = 2 \text{ GeV}/c$ (dashed line in the lower panel of Fig. 5). We expect the non-monotonicity of $v_2(p_T)$ to persist to larger p_T values for protons whose low- p_T spectra are more strongly affected by radial flow than those of pions (see Fig. 2). Figure 6 supports this expectation by showing that for protons (in contrast to pions) the differential elliptic flow at the LHC is *smaller* than at RHIC over the entire p_T -range shown in that Figure.

It is important to note, however, that, while the differential elliptic flow at fixed p_T *decreases* between RHIC and LHC energies, the total momentum anisotropy, reflected by the p_T -integrated elliptic flow coefficient v_2 , *increases* from RHIC to LHC. Radial flow flattens the LHC spectra dramatically, putting a larger weight on the larger v_2 values at higher p_T , and as a result the p_T -integrated elliptic flow is larger at the LHC, even though at any fixed p_T value below $1 \text{ GeV}/c$ it is smaller than at RHIC. This is shown in the upper panel of Fig. 5 for both directly emitted pions (dashed line) and all pions including resonance decay contributions (solid line). Again, one sees first a rise of v_2 at low \sqrt{s} (AGS energies), followed by a decrease between SPS and RHIC and another rise between RHIC and LHC [7]. The non-monotonicity of the p_T -integrated v_2 can be related to the quark-hadron phase transition and the corresponding softening of the EOS in the transition region [7]. In the experimental data this phase transition signature is, unfortunately, washed out by strong viscous effects in the late hadronic stage of the fireball expansion which become increasingly important at low collision energies [11,12,18] (where the fireball spends most of its time in the hadronic phase). As a result, the experimentally measured integrated elliptic flow v_2 rises monotonically with \sqrt{s} , approaching the ideal fluid limit only at or above RHIC energies [21].

The upper panel of Fig. 5 shows that at all collision energies the directly thermally emitted pions show more p_T -integrated elliptic flow than all pions together. From this we can deduce that pions emitted from resonance decays have a lower momentum anisotropy. This is at least partially understood by the fact that decay pions typically have smaller transverse momenta than their parent resonances [31], and that the parent resonances, being heavier, contribute less elliptic flow at low p_T than pions (see Fig. 6) [36].

Comparison of the curves shown in the upper panel of Fig. 5 with those in the right panel of Fig. 2 in Ref. [21] shows that in a hybrid model approach (which includes viscous effects

in the hadronic phase) the p_T -integrated elliptic flow increases by about 25% between RHIC and LHC whereas in the ideal fluid approach (which neglects hadronic viscosity) it increases by less than 10%. The largest contribution to the expected increase of v_2 from RHIC to LHC is therefore due to the *disappearance* of late hadronic viscous effects between RHIC and LHC because the fireball spends a smaller fraction of its time in the hadronic phase and the elliptic flow saturates before the QGP converts to hadrons.

5 Conclusions

We have shown that, while the radial flow and the p_T -integrated elliptic flow *increase* from RHIC to LHC, the differential elliptic flow at fixed $p_T < 1.5 \text{ GeV}/c$ *decreases* in the same collision energy range. This decrease of $v_2(p_T)$ is driven by a (relative) depletion of low p_T hadrons by radial flow which pushes the hadrons to larger transverse momenta. The observed “saturation” of $v_2(p_T)$ seen by PHENIX [17] between $\sqrt{s} = 63$ and 200 GeV likely signals the onset of this kinematic effect and should thus not be interpreted without further scrutiny as a signature for the quark-hadron phase transition.

When experimental data will become available for very high energy collisions at the LHC, the ideal fluid dynamical calculations presented here can serve as a benchmark for comparison with experiment, providing insights into the validity of ideal hydrodynamics at high energy densities and permitting quantification of deviations from ideal fluid behaviour. This should facilitate the discovery of possible novel effects, beyond those expected from collective dynamics, at LHC energies.

Acknowledgements: We thank Rupa Chatterjee, Evan Frodermann, Richard Furnstahl and Huichao Song for helpful comments. The work of G.K. was supported by the National Science Foundation under grant PHY-0354916, that of U.H. by the U.S. Department of Energy under contract DE-FG02-01ER41190.

References

1. P. Huovinen, in *Quark-Gluon Plasma 3*, edited by R. C. Hwa and X.-N. Wang (World Scientific, Singapore, 2004), p. 600 [arXiv:nucl-th/0305064].
2. P. F. Kolb and U. Heinz, in *Quark-Gluon Plasma 3*, edited by R. C. Hwa and X.-N. Wang (World Scientific, Singapore, 2004), p. 634 [arXiv:nucl-th/0305084].
3. P. Huovinen and P. V. Ruuskanen, *Ann. Rev. Nucl. Part. Sci.* **56** (2006) 163.
4. I. Arsene *et al.* [BRAHMS Collaboration] *Nucl. Phys. A* **757**, 1 (2005); B.B. Back *et al.* [PHOBOS Collaboration], *Nucl. Phys. A* **757**, 28 (2005); J. Adams *et al.* [STAR Collaboration], *Nucl. Phys. A* **757**, 102 (2005); K. Adcox *et al.* [PHENIX Collaboration], *Nucl. Phys. A* **757**, 184 (2005).
5. J. Hofmann, H. Stöcker, U. Heinz, W. Scheid and W. Greiner, *Phys. Rev. Lett.* **36** (1976) 88; H. Stöcker and W. Greiner, *Phys. Rept.* **137** (1986) 277.
6. D. H. Rischke, Y. Pürsün, J. A. Maruhn, H. Stöcker and W. Greiner, *Heavy Ion Phys.* **1** (1995) 309.
7. P. F. Kolb, J. Sollfrank and U. Heinz, *Phys. Lett. B* **459** (1999) 667; and *Phys. Rev. C* **62** (2000) 054909.
8. J. Brachmann *et al.*, *Phys. Rev. C* **61** (2000) 024909.
9. P. Huovinen, *Nucl. Phys. A* **761** (2005) 296.
10. F. Karsch and E. Laermann, in *Quark-Gluon Plasma 3*, edited by R. C. Hwa and X.-N. Wang (World Scientific, Singapore, 2004), p. 1 [arXiv:hep-lat/0305025].
11. D. Teaney, J. Lauret and E. V. Shuryak, arXiv:nucl-th/0110037.
12. T. Hirano, U. Heinz, D. Kharzeev, R. Lacey and Y. Nara, *Phys. Lett. B* **636** (2006) 299.
13. C. Alt *et al.* [NA49 Collaboration], *Phys. Rev. C* **68** (2003) 034903.
14. S. A. Voloshin, *J. Phys. G: Nucl. Part. Phys.* **34** (2007) S883; and AIP Conf. Proc. **870** (2006) 691 [arXiv:nucl-ex/0610038].
15. G. Torrieri, *Phys. Rev. C* **76** (2007) 024903.
16. H. Song and U. Heinz, *Phys. Rev. C* **78** (2008) 024902.
17. S. S. Adler *et al.* [PHENIX Collaboration], *Phys. Rev. Lett.* **94** (2005) 232302.

18. U. Heinz, J. Phys. G: Nucl. Part. Phys. **31** (2005) S717.
19. U. Heinz, J. Phys. Conf. Ser. **50** (2006) 230.
20. R. A. Lacey, N. N. Ajitanand, J. M. Alexander, P. Chung, J. Jia, A. Taranenko and P. Danielewicz, arXiv:0708.3512 [nucl-ex].
21. T. Hirano, U. Heinz, D. Kharzeev, R. Lacey and Y. Nara, J. Phys. G: Nucl. Part. Phys. **34** (2007) S879.
22. K. J. Eskola, H. Honkanen, H. Niemi, P. V. Ruuskanen and S. S. Räsänen, Phys. Rev. C **72** (2005) 044904.
23. H. Niemi, K. J. Eskola and P. V. Ruuskanen, arXiv:0806.1116 [hep-ph].
24. P. F. Kolb and R. Rapp, Phys. Rev. C **67** (2003) 044903.
25. AZHYDR0 can be downloaded from URL <http://nt3.phys.columbia.edu/people/molnard/OSCAR/>.
26. T. Hirano and K. Tsuda, Phys. Rev. C **66** (2002) 054905.
27. D. Teaney, arXiv:nucl-th/0204023.
28. J. I. Kapusta, L. D. McLerran and D. K. Srivastava, Phys. Lett. B **283** (1992) 145.
29. B.B. Back *et al.* [PHOBOS Collaboration], Nucl. Phys. **A757** (2005) 28 and Phys. Rev. C **74** (2006) 021902(R); W. Busza, J. Phys. G **35** (2008) 044040.
30. E. Schnedermann, J. Sollfrank and U. W. Heinz, Phys. Rev. C **48** (1993) 2462.
31. U. Heinz, *Concepts of Heavy-ion Physics*, Lectures presented at the *2nd Latin American School of High-Energy Physics*, San Miguel Regla, Mexico, 1-14 June 2003. CERN Yellow Report CERN-2004-001 (N. Ellis and R. Fleischer, eds.), p. 165-238 [arXiv:nucl-th/0407360].
32. N. Armesto *et al.*, J. Phys. G: Nucl. Part. Phys. **35** (2008) 054001.
33. H. B. Meyer, Phys. Rev. D **76** (2007) 101701.
34. P. Huovinen, private communication.
35. P. Huovinen, P. F. Kolb, U. Heinz, P. V. Ruuskanen and S. A. Voloshin, Phys. Lett. B **503** (2001) 58.
36. T. Hirano, Phys. Rev. Lett. **86** (2001) 2754.